http://dx.doi.org/10.21172/ijiet.82.006

Structural and Dielectric properties of Co^{+2} substituted Ni Cu Nanocrystalline Spinel Ferrite Material

A.M. Tamboli
Department of Electronic Science, Poona College, Camp, Pune-411 001 INDIA.

S.M. Rathod
Department Of Physics, Abasaheb Garware College, Pune- 411 004 INDIA

Gulam Rabbani
Department of Physics and Electronics, Maulana Azad College, Aurangabad-431 001 INDIA

Abstract: In this research paper the dielectric properties such as Ddielectric loss (tan δ), AC conductivity, Dielectric constant (real part ε' and imaginary part ε") and dielectric loss tangent (tan δ) are reported for the series [Cox Ni(constant) Cu0.8-x Fe2O4] where constant=0.2 with x=0.2, 0.4 and 0.6 of ferrites, prepared by Sol-Gel auto-combustion technique by using high purity metal nitrate, double distilled water and citric acid as a catalyst. The variation in the real part of dielectric constant(ε') , imaginary part of dielectric constant (ε") , dielectric loss tangent (tan δ)and AC conductivity are studied at room temperature in the frequency range of 100 Hz to 5 MHz. Structural characterization of the annealed samples was done with the help of X-ray diffraction method. The particle size and single phase formation of CoNiCuFe2O4 ferrite was confirmed by X-ray diffraction analysis. The particle size of prepared sample was confirmed by Scherer's formula. The effect on Particle size (t) and lattice constant (Å) is observed due to substitution of Co2+ in Ni Cu. The impedance meter (LCR meter) is used to obtain the Dielectric properties of prepared pallets. The variations in the structural and dielectric properties of the prepared ferrite material are discussed.

Keywords – Sol-gel auto-combustion X-ray diffraction, Impedance meter (LCR meter), FT-IR,

I. INTRODUCTION

The ferrite nanoparticle are popular in various fields of electronics and communication Engineering because the ferrite material is having excellent and very different properties especially in electric, di-electric and magnetic properties that are sensibly different from the properties of the other bulk materials. Ferrite nanoparticles are very use full in the area where minimization of eddy current loss, magnetic loss is important and magnetic field dependent properties plays very important role.
The ferrite performs a better response at high frequencies because ferrite nanoparticles are having very high electrical resistivity and due to this Ferrite is used as best core material in the transformers and power supply for frequencies from few kilo Hertz to a few Mega Hertz. Ferrite is having high stability, low cost, light weight and lowest volume therefore it is more popular. These are intensively studied due to their technological applications in microwave industries such as Radar Absorbing Material (RAM), satellite communication, microwave dark room and protection of living animals from the harm of microwave [1–7].

II. EXPERIMENTAL

2.1 Synthesis

The high purity AR grade ferric nitrate [$Fe(NO_3)_3.9H_2O$)], Copper nitrate [Cu $(NO_3)_2$ $.6H_2O$], Nickel nitrate [$Ni(NO_3)_2.6H_2O$],Cobalt nitrate [$Co(NO_3)_2.6H_2O$], citric acid ($C_6H_8O_7$), ammonium hydroxide solution (NH_4OH) and double distilled water were used to prepare the series [Co_x Ni(constant) $Cu_{0.8-x}$ Fe_2O_4] where constant=0.2 with x=0.2, 0.4 and 0.6 of ferrite nanoparticles by sol-gel auto combustion synthesis technique. In this chemical process Citric acid was used as a Fuel. These nitrates and citric acid were weighed accurately to have proper stoichiometric proportion required in the final product and all metal nitrates are dissolved in deionized water to form mixed solution. The mixed solutions of all the chemicals were stirred by using magnetic stirrer until the homogeneous solution is obtained. During the stirring process ammonium hydroxide solution was added drop by drop to obtain pH of 7. The mixed solution was simultaneously heated at 100 $^{\circ}$C for 2 hours

http://dx.doi.org/10.21172/ijiet.82.006

to 4 hours such that formation of gel takes place. The transparent solution was heated at 100°C for 2 hours to 4 hours for removal of water and solution turns into a viscous brown gel. The temperature of the gel was further increased up to 150 °C, after some time combustion of the gel takes place and fine powder of [Co_x Ni(constant) $Cu_{0.8-x}$ Fe_2O_4] ferrite nanoparticle was obtained. The same procedure is repeated for three times for X=0.2, x=0.4 and x=0.6, such that three ferrite materials are prepared. Three ferrite materials represented by the symbol D, E, and A are [$(Co_{0.2}Ni_{.0.2}\,Cu_{.0.6})Fe_2O_4$], [$(Co_{0.4}Ni_{.0.2}\,Cu_{.0.4})Fe_2O_4$] and [$(Co_{0.6}Ni_{.0.2}\,Cu_{.0.2})Fe_2O_4$] respectively.
The powder was dried and annealed at 400 °C for 4h in furnace having super kanthal ($MoSi_2$) heating elements and alumina insulation boards as chamber walls. The pallets of sample are prepared by using binder polyvinyl alcohol (PVA) and it was pressed at 60 kg/cm^3 for one min and was dried and annealed at 200 °C for 2 hours. The diameter of pallet is 10mm and thickness is 2mm. Three pallets of ferrite materials are prepared for represented by D, E, and A are [$(Co_{0.2}Ni_{.0.2}\,Cu_{.0.6})Fe_2O_4$], [$(Co_{0.4}Ni_{.0.2}\,Cu_{.0.4})Fe_2O_4$] and [$(Co_{0.6}Ni_{.0.2}\,Cu_{.0.2})Fe_2O_4$] respectively.

2.2 Characterization

The phase analysis and gross structural analysis is done by using X-ray diffractometer (Cu $K\alpha_1$ radiation=1.5418 Å) and confirmation of single phase spinal structure is done. The average particle size of prepared powder has been calculated using Scherrer formula

$$t = 0.9\,\lambda / \beta \cos\theta \qquad \text{----------(1)}$$

Where; λ = Wave length of X-rays.
t = Particle size.
θ = Bragg's angle.
β = Full Width Half Maxima of the recorded peak θ and it is corrected for instrumental broadening.

The lattice parameter (a) is calculated from X-ray diffraction data by using formula $1/d^2 = 1/a^2 * (h^2 + k^2 + l^2)$. It is observe that Average Grain Size t (nm) and Lattices Constant a (Å) decreases with increase of Ni^{2+} substitution of in Cu Co as shown in Table 1.

The dielectric constant (ε') , dielectric loss tangent (tan δ) and AC conductivity (σ_{ac}) of prepared samples were measured in the frequency range of 100 Hz to 5 MHz by using digital LCR meter of precision impedance analyser at room temperature. The data of digital LCR meter provides the information of frequency (f), Series Capacitance (Cs), Parallel Capacitance (Cp), Quality factor (Q) , by using the this date along with thickness of pellet, d=0.002 meter, Diameter of pellet= 10 millimetre and Area of pellet = πr^2 = 3.14*.005*.005 meter^2=0.0000785 meter^2, the calculations for dielectric constant (ε') , imaginary part (ε") of dielectric constant and dielectric loss tangent (tan δ) are completed by using the following equations. The logarithm of frequency (Log_{10} f) is taken in to consideration while plotting the graph of (Log_{10} f) verses any other parameter.

$$\text{Dielectric constant (Real Part)} = \acute{\varepsilon} = Cp*d/\varepsilon_0*A \qquad \text{---------- (2)}$$
$$\text{Dielectric constant (Imaginary Part)} = \varepsilon'' = (\tan\delta)*\varepsilon' \qquad \text{---------- (3)}$$
$$\text{Dielectric loss tangent= } (\tan\delta) = 1/Q = \varepsilon''/\varepsilon' \qquad \text{---------- (4)}$$

III. RESULTS AND DISCUSSIONS

3.1: Structural analysis.

The XRD pattern of as-synthesized ferrite material of [$(Co_{0.2}Ni_{.0.2}\,Cu_{.0.6})Fe_2O_4$] is shown in Fig.1. The highest intensity peaks in all three specimens are observed at (311) and other peaks (220), (400), (422) and (440). The average grain (crystallite) size for all the composites is calculated using Scherer's formula with respect to the high intense peak plane (311) and Lattices Constant a (Å) is calculated by using the formula $1/d^2 = 1/a^2 * (h^2 + k^2 + l^2)$. It is observed that due to the increase concentration of Co^{2+} ions in NiCu the Bragg's angle shifts towards lower angle and thereby interplaner spacing's (d) values increases. The grain (crystallite) size for all the composites is found in the range of 23.71 nanometer to 28.45 nanometer. The XRD pattern contains no secondary peaks and it gives the confirmation about pure spinal structure of sample.

The lattice constant is found to increase with increase in Co^{2+} concentration x. The variations in lattice constant as a function of Cobalt concentration x can be understood on the basis of the ionic radius of the substituted cations. Since the ionic radius of Co^{2+} ions (0.745Å) is greater than that of Cu^{2+} ions (0.73Å), the substitution is expected to increase the lattice constant with increase in cobalt concentration x. When the larger cobalt ions enters at that time lattice unit cell expands while preserving overall symmetry this is true as long as the lattice constant increases with substituent concentration of cobalt.

The values of lattice constant obtained from XRD data by varying cobalt concentration x are given in Table 1. It can be seen from Table 1 that, the lattice constant and particle size (t) increases with increase of cobalt concentration x and obeys Vegard's law [08-14]. Fig.2. Shows that particle size (t) increases with

http://dx.doi.org/10.21172/ijiet.82.006

increase of Co^{2+} concentration in $[(Co_x\ Ni_{(constant)}\ Cu_{0.8-x})Fe_2O_4]$ and Fig.3. Shows that lattice constant (Å) also increases with increase of Co^{2+} concentration in $[(Co_x\ Ni_{(constant)}\ Cu_{0.8-x})Fe_2O_4]$.

3.2: Dielectric properties.

The effect of Co^{2+} concentration x on the dielectric properties of $[(Co_{0.2}Ni_{.0.2}\ Cu_{.0.6})Fe_2O_4]$, $[(Co_{0.4}Ni_{.0.2}\ Cu_{.0.4})Fe_2O_4]$ and $[(Co_{0.6}Ni_{.0.2}\ Cu_{.0.2})Fe_2O_4]$ have been studied by using LCR meter (impedance analyzer) in frequency range of 100 Hz–5 MHz.

The Fig. 4 shows that the dielectric loss (tan δ) decreases as the frequency of the applied AC electric field increases because the jumping frequency of charge carriers cannot follow the frequency of the applied field after certain frequency. It is also observed that dielectric loss (tan δ) rapidly decreases at lower frequencies and remains constant at higher frequencies.

The Zig Zag behaviour in the low frequency region of Dielectric loss curve is observed as shown in Fig. 4. This peak in the Dielectric loss curve is observed when the hopping frequency of the electron between Fe^{2+} –Fe^{3+} ions matches with the frequency of the externally applied electric field. It is expected that the peak may be observable in lower frequency range.

The Fig. 5 shows that the variation in the dielectric constant (έ) with increase in the frequency and it is observed that dielectric constant (έ) of all spinel ferrite samples rapidly decreases at lower frequencies and remains constant at higher frequencies.

The Fig. 6 shows that the Imaginary Part of Dielectric constant (ε″) also decreases rapidly at lower frequency and remains constant at higher frequencies. Similar results were observed by several other investigators [15-19]. The values of the average dielectric constant and average dielectric loss of the samples are listed in Table 2.

According to Koop's the decrease in dielectric constant for increase in frequency can be expressed by considering the solid as composed of well conducting grains which is separated by the poorly conducting grain boundaries**.** According to Koop's, at lower frequencies, the resistivity is high and the principal effect is of the grain boundaries (low resistivity regions). Therefore, the energy required for electron hopping between Fe^{2+} and Fe^{3+} at the grain boundaries is higher and the energy losses (tan δ and ε″) are larger [20-25].

The rapid decrease of dielectric constant at lower frequencies is explained on the basis of space charge polarization. According to Maxwell and Wagner two-layer model, the space charge polarization is produced in a di-electric material due to the presence of higher conductivity phases (grains) in the insulating matrix (grain boundaries). When an external electric field is applied, the electrons reach the grain boundary through hopping. If the resistance of the grain boundary is high, the electrons pile up at the grain boundaries and produces polarization. This is called space charge polarization. The assembly of space charge carriers in a dielectric material takes a finite time to line up their axes parallel to the alternating electric field. If the frequency of the external electric field reversal increases, a point is reached where the space charge carriers cannot keep up with the external electric field and the alternation of their direction lags behind that of the field [26-29]. In Fig. 7, FT-IR peaks at 3148.22 cm^{-1}, 2983.34 cm^{-1},1644.98 cm^{-1} and 1024.02 cm^{-1} gives the confirmation of Fe_2O_4.

3.3: AC conductivity (σ) at different concentration of Co^{2+} ions.

It is observed that the AC conductivity remains almost constant in the low frequency region and increases abruptly in the high frequency region Fig. 8. It is well known that the mechanism of the electrical conduction is the same as that of the dielectric polarization.

The increase in the AC conductivity with frequency is also understood by the hopping model. As the frequency of the applied electric field increases, the hopping frequency of electrons between Fe^{3+} –Fe^{2+} ions at adjacent octahedral site also increases, leading to increase in the conductivity.

From Fig. 8. it is observed that for x=0.2 (sample D) graph shown by square dots (Black) is having the minimum AC Conductivity and AC Conductivity increases due increase in substation of Co^{2+}, x=0.4 and x=0.6 which is shown by circular red dots (sample E) and by triangular blue dots (sample A) respectively.

It shows that the AC conductivity increases with increase in x substitution of Co^{2+}. With the increase in the concentration of Co^{2+} ions (x), the hopping action of charge carriers increases due to the increased concentration of Fe^{3+} ions at B-site. Table 3, shows the values of AC Conductivity for Co^{2+} concentration x at 5 MHz [30-34].

IV. FIGURES AND TABLES

Table 1

http://dx.doi.org/10.21172/ijiet.82.006

Variation of Particle size (t) and Lattices Constant (Å) for due to Substitution of Co^{2+} in $[(Co_xNi_{(constant)}\,Cu_{0.8-x})Fe_2O_4]$.

Ferrite Sample	Particle Size t (nm)	Lattices Constant (Å)
(D) x=0.2	23.71	8.315
(E) x=0.4	25.75	8.377
(A) x=0.6	28.45	8.417

Table 2
Variation of Dielectric Constant and Dielectric loss of $[(Co_xNi_{(constant)}\,Cu_{0.8-x})Fe_2O_4]$.

Variation in Dielectric Constant and Dielectric loss of D, E and A		
Sample Name	Avg. Dielectric Constant	Avg. Dielectric loss
D $[(Co_{0.2}\,Ni_{.0.2}\,Cu_{.0.6})Fe_2O_4]$	40.372577	1.191974
E $[(Co_{0.4}Ni_{.0.2}\,Cu_{.0.4})Fe_2O_4]$	88.997411	1.342013
A $[(Co_{0.6}\,Ni_{.0.2}\,Cu_{.0.2})Fe_2O_4]$	52.907096	0.701638

Table 3
Variation in AC Conductivity of $[(Co_xNi_{(constant)}\,Cu_{0.8-x})Fe_2O_4]$.

$[Co_x\,(Ni_{(constant)}\,Cu_{0.8-x})Fe_2O_4]$, Ni =constant=0.2	
x	AC Conductivity at 5 MHz
(D) For x=0.2	0.00206424
(E) For x=0.4	0.00259871
(A) For x=0.6	0.00265852

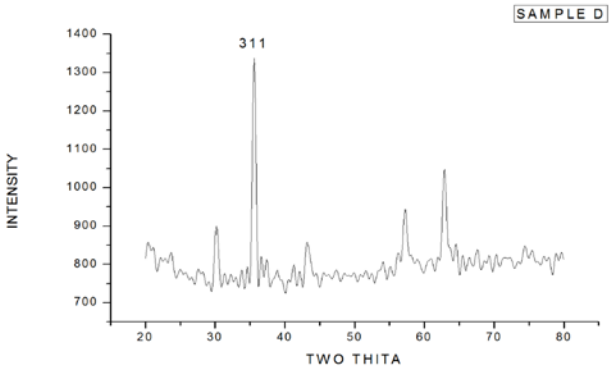

Fig.1: XRD pattern of sample D , $[(Co_{0.2}Ni_{.0.2}\,Cu_{.0.6})Fe_2O_4]$.

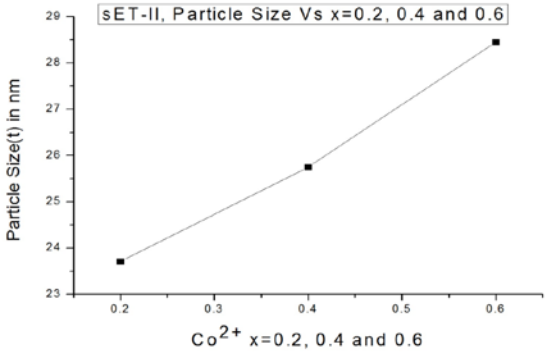

Fig. 2: Particle size (t) verses Co^{2+} substitution x in SET-II (D, E, A).

http://dx.doi.org/10.21172/ijiet.82.006

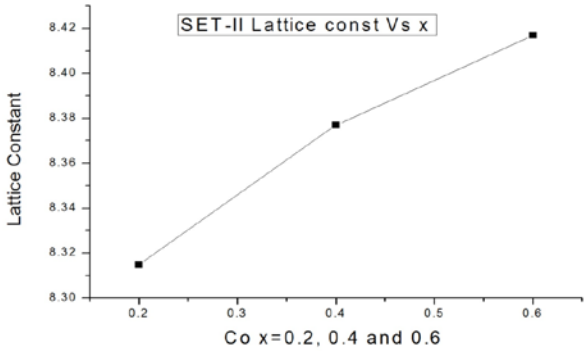

Fig. 3: Lattices Constant verses Co^{2+} substitution x in SET-II (D, E, A).

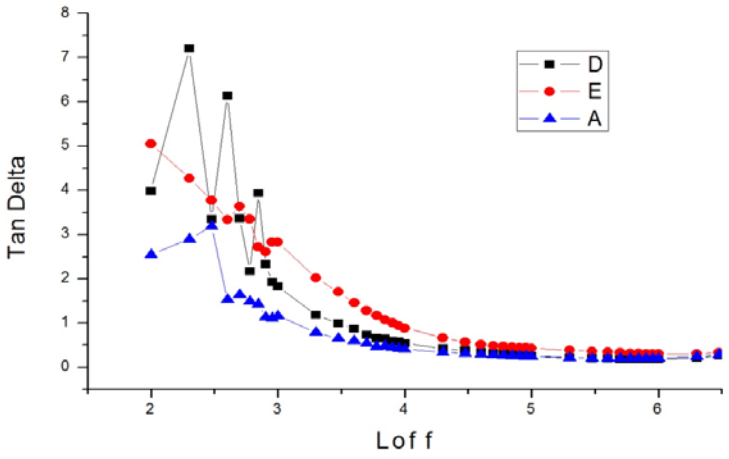

Fig. 4: Variation in dielectric loss (tan δ) with increase in frequency of ferrite sample D, E and A.

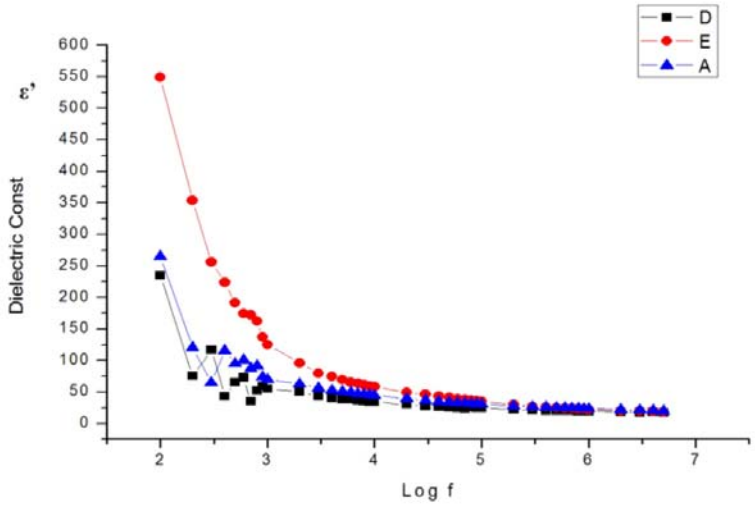

Fig. 5: Variation in Real Part of Dielectric constant (έ) with increase in frequency of ferrite sample D, E and A.

http://dx.doi.org/10.21172/ijiet.82.006

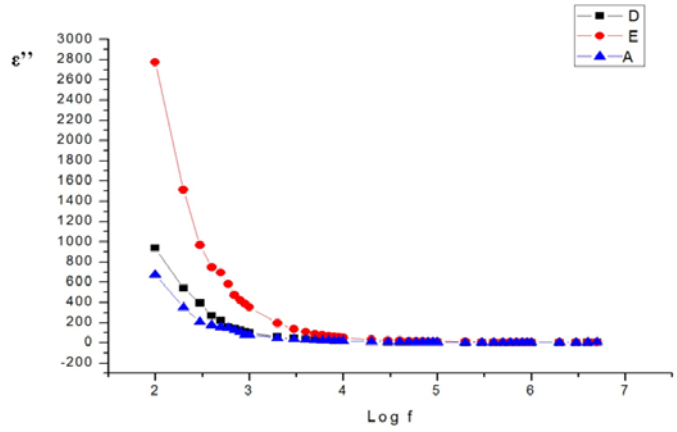

Fig. 6: Variation in imaginary part of Dielectric Constant (ε″) with increase in frequency of ferrite sample D, E and A.

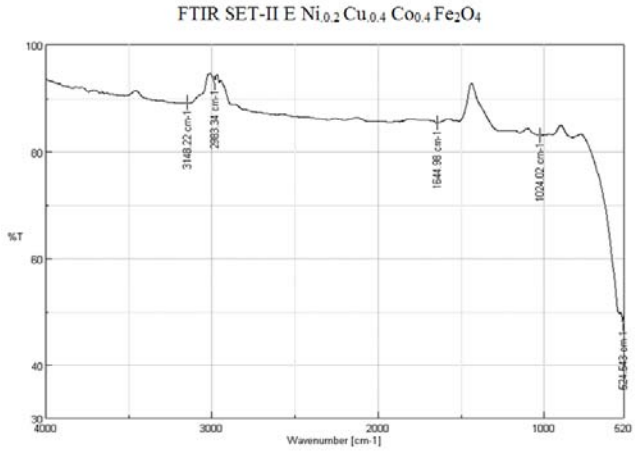

Fig.7: FTIR graph for SET-II (E), [($_4$Co$_{0.4}$Ni$_{0.2}$ Cu$_{0.}$) Fe$_2$O$_4$]

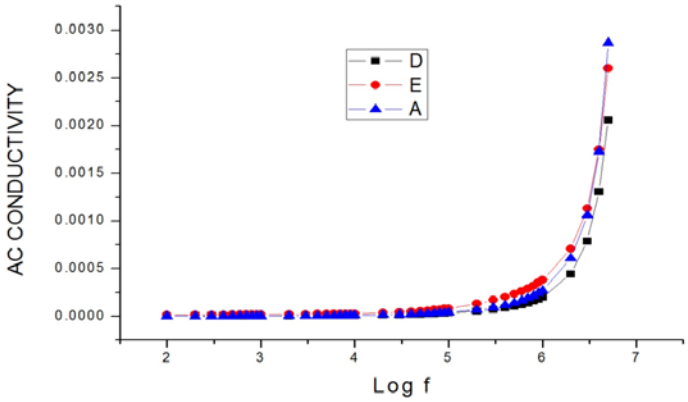

Fig. 8: AC Conductivity of ferrite sample D, E and A.

V. CONCLUSIONS

The nanocrystalline ferrite samples [($Co_{0.2}Ni_{0.2}$ $Cu_{0.6}$)Fe_2O_4], [($Co_{0.4}Ni_{0.2}$ $Cu_{0.4}$)Fe_2O_4] and [($Co_{0.6}Ni_{0.2}$ $Cu_{0.2}$)Fe_2O_4] have been successfully prepared by sol-gel auto combustion technique. All the prepared samples show the single phase cubic spinel structure of the samples. The particle grain size obtained from X-ray diffraction data increases with increase in Co^{+2} substitutions **Ni** Cu. It clearly shows that the size of the ferrite particles was in the nanometer range. The particle size and nanostructure of the sample was examined by XRD. FTIR also gives the confirmation of spinnel ferrite. Measurement of the dielectric constant and dielectric loss in the 100 Hz–5 MHz frequency range showed higher magnitude, at lower frequencies, decreasing with increase in frequency, essentially becoming constant above 4 MHz. The AC conductivity (σ) increases with increase in x substitution of Co^{2+}.

REFERENCES

[01] Y.-L. Liu, Z.-M. Liu, Y. Yang, H.-F. Yang, G.-L. Shan, R.-Q. Yu, Simple synthesis of $MgFe_2O_4$ as gas sensing materials, Sens. *Actuat. B 107 (2005)* 600–604.
[02] C.V. Gopal Reddy, S.V. Manorama, V.J. Rao, Preparation and characterization of ferrite as gas sensor materials, *J. Mater. Sci. Lett. 19* (2000) 775.
[03] N. Xinshu, L. Yanli, X. Jiaqiang, Simple synthesis of $MgFe_2O_4$ as gas sensing materials, *Chin. Funct. Mater.* 33 (2002) 413.
[04] L. Satyanarayana, K. Madhusudan Reddy, V.M. Sankara, Nanocrystalline spinel $Ni_{0.6}Zn_{0.}4Fe_2O_4$: *a novel materials for H_2S, Mater. Chem. Phys.* 82 (2003) 21.
[05] G.F. Goya, H.R. Rechenberg, Superparamagnetic transition and local-order in $CuFe_2O_4$ nanoparticles, *Nanostruct. Mater.* 10 (1998) 1001–1011.
[06] J.Z. Jiang, G.F. Goya, H.R. Rechenberg, Magnetic properties of nanostructured $CuFe_2O_4$, *J. Phys. Condens. Mater.* 11 (1999) 4063–4078.
[07] P.B. Pandya, H.H. Joshi, R.G. Kulkarni, Magnetic and structural properties of $CuFe_2O_4$, prepared by co-precipitation method, *J. Mater. Sci. Lett.* 10 (1991) 474–476.
[08] A.T.Raghavendar, Damir Pajic, Kreso Zadro, Tomislav Milekovic, P. Vekateshwar Rao, K.M. Jadhav, D. Ravinder, *J. Magn.Magn.Mater.* 3 (2007) 204.
[09] C. G. Whinfrey, D. W. Eckort and A. Tauber, *J. Am. Chem. Soc.* 53 (1982) 2722
[10] C. Caizer, M. Stefanescu, *J. Phys. D. Appl. Phys.*35 (2002) 3035.
[11] M.A. Ahmed, S.F. Mansour, M. Afifi, *J. Magn. Magn. Mater.* 324 (2012) 4-10.
[12] P.S. Aghav, V.N. Dhage, M.L. Mane, D.R. Shengule, R.G. Dorik, K.M. Jadhav, *Physica B: Cond. Matter*. 406(2011) 4350
[13] J. Jing, L. Liangchao, X. Feng, *J. Rare Earths* 25 (2007) 79.
[14] S. Sun, C.B. Murray, D. Weller, L. Folks, A. Moser, Monodisperse FePt nanoparticles and ferromagnetic FePt nanocrystal superlattices, *Science 287* (2000) 1989.
[15] I.H. Gul, W. Ahmed, A. Maqsood, Electrical and magnetic characterization of nanocrystalline Ni–Zn ferrite synthesis by co-precipitation route, *J. Magn. Magn. Mater.* 320 (2008) 270–275.
[16] M.U. Islam, T. Abbas, Shahida B. Niazi, Zubair Ahmad, Sadia Sabeen, M. Ashraf Chaudhry, Electrical behaviour of fine particle co-precipitation prepared Ni–Zn ferrites, *Solid State Commun.* 130 (2004) 353–356.
[17] J. Smit, H.P.J. Wijn, Ferrites, in: *Phililps Technical Library, Eindhovan, Netherlands*, 1959, pp. 221–245.
[18] B.D. Cullity, in: *Elements of X-ray Diffraction, second ed., Addison Wesley Pub. Co. Inc*., 1978.
[19] A. Verma, R. Chatterjee, Effect of zinc concentration on the structural, electrical and magnetic properties of mixed Mn–Zn and Ni–Zn ferrites synthesized by the citrate precursor technique, *J. Magn. Magn. Mater.* 306 (2006) 313–320.
[20] T. Nakamura, Y. Okaro, Electromagnetic properties of Mn–Zn ferrite sintered ceramics, *J. Appl. Phys.* 79 (1996) 7129.
[21] A. Verma, T.C. Geol, R.G. Mendiratta, Magnetic properties of nickel–zinc ferrites prepared by the citrate precursor method, *J. Magn. Magn. Mater.* 210 (2000) 274.
[22] L.G. Van Uitert, DC resistivity in the nickel and nickel zinc ferrite system, *J Chem. Phys.* 23 (10) (1955) 1883.
[23] C. Heck, in: *Magnetic Materials and their Applications, Butterworths, London,* 1974 506.
[24] M.R. Anantharaman, S. Sindhu, S. Jagatheesan, K.A. Malini, P. Kurian, Dielectric properties of rubber ferrite composites containing mixed ferrites, *J Phys.* D 32 (1999) 1801.
[25] T.Jahanbin, M. Hashim, K. A. Mantori, Comparative studies on the structure and electromagnetic properties of Ni-Zn ferrites prepared via co-precipitation and conventional ceramic processing routes, *J. Magn. Magn. Mater.* 322(2010) 2684-2689.
[26] C.G. Koops, On the dispersion of resistivity and dielectric constant of some semiconductors at audio frequencies, *Phys. Rev.* 83 (1951) 121.
[27] J S. Upadhyay, S. Devendrakumar, S. Omprakash, Effect of compositional variation on dielectric and electrical properties of $Sr_{1-x}La_xTi_{1-x}Co_xO_3$ system, *Bull. Mater. Sci.* 19 (1996) 513.
[28] A. Verma, T.C. Goyal, R.G. Mendiratta, M.I. Alam, Dielectric properties of NiZn ferrites prepared by the citrate precursor method, *Mater. Sci. Eng.* B60 (1999) 156–162.
[29] H. Hsiang, W.S. Chen, Y.L. Chang, F.C. Hsu, F.S. Yen, Ferrite load properties of NiZn ferrite powders-epoxy resin coatings, Am. *J. Mater. Sci.* 1 (2011) 40–44.
[30] K.W. Wagner, *Ann. Phys.* 40 (1913) 817.
[31] I.T. Rabinkin, Z.I. Novikova, *Ferrites, Izv Acad. Nauk USSR, Minsk*, 1960.
[32] J.C. Maxwell, Electricity and Magnetism, *vol. 1, Oxford University Press, New York* (1973), p. 1.
[33] M. Penchal Reddy, W. Madhuri, N. Ramamanoher Reddy, K.V. Siva Kumar, V.R.K. Murthy, R. Ramakrishna Reddy, Influence of copper substitution on magnetic and electrical properties of MgCuZn ferrite prepared by microwave sintering method, *Mater. Sci. Eng.* C 30 (2010) 1094–1099.
[34] J. Azadmanjiri, H.K. Salehani, M.R. Barati, F. Farzan, Preparation and electromagnetic properties of $Ni_{1-x}Cu_xFe_2O_4$ nanoparticle ferrites by sol–gel auto-combustion method, *Mater. Lett.* 61 (2007) 84–87.